

Clustering and lifetime of Lyman Alpha Emitters in the Epoch of Reionization

Anne Hutter^{1*}, Pratika Dayal², Volker Müller¹

¹ *Leibniz-Institut für Astrophysik, An der Sternwarte 16, 14482 Potsdam, Germany*

² *Institute for Computational Cosmology, Department of Physics, University of Durham, South Road, Durham DH1 3LE, UK*

ABSTRACT

We calculate Lyman Alpha Emitter (LAE) angular correlation functions (ACFs) at $z \simeq 6.6$ and the fraction of lifetime (for the 100 Myrs preceding $z \simeq 6.6$) galaxies spend as Lyman Break Galaxies (LBGs) or as LBGs with Lyman Alpha ($\text{Ly}\alpha$) emission using a model that combines SPH cosmological simulations (GADGET-2), dust attenuation and a radiative transfer code (pCRASH). The ACFs are a powerful tool that significantly narrows the 3D parameter space allowed by LAE $\text{Ly}\alpha$ and UV luminosity functions (LFs) alone. With this work, we simultaneously constrain the escape fraction of ionizing photons $f_{\text{esc}} = 0.05 - 0.5$, the mean fraction of neutral hydrogen in the intergalactic medium (IGM) $\langle \chi_{\text{HI}} \rangle \lesssim 0.01$ and the dust-dependent ratio of the escape fractions of $\text{Ly}\alpha$ and UV continuum photons $f_{\alpha}/f_c = 0.6 - 1.2$. Our results show that reionization has the largest impact on the amplitude of the ACFs, and its imprints are clearly distinguishable from those of f_{esc} and f_{α}/f_c . We also show that galaxies with a critical stellar mass of $M_* = 10^{8.5} (10^{9.5}) M_{\odot}$ produce enough luminosity to stay visible as LBGs (LAEs). Finally, the fraction of time during the past 100 Myrs prior to $z = 6.6$ a galaxy spends as a LBG or as a LBG with $\text{Ly}\alpha$ emission increases with the UV magnitude (and the stellar mass M_*): considering observed (dust and IGM attenuated) luminosities, the fraction of time a galaxy spends as a LBG (LAE) increases from 65% to 100% ($\simeq 0 - 100\%$) as M_{UV} decreases from $M_{UV} = -18.0$ to -23.5 (M_* increases from $10^8 - 10^{10.5} M_{\odot}$). Thus in our model the brightest (most massive) LBGs most often show $\text{Ly}\alpha$ emission.

Key words: radiative transfer - methods: numerical - dust, extinction - galaxies: high-redshift - dark ages, reionization, first stars

1 INTRODUCTION

The Epoch of Reionization (EoR) marks a major phase change in the ionization state of the Universe. While the intergalactic medium (IGM) is predominantly composed of neutral Hydrogen (H I) at the beginning of this epoch, it is completely ionized by the end, as a result of H I ionizing photons produced by both stars and quasars. However, the progress of reionization has been hard to pin down since it depends on a number of parameters including the initial mass function (IMF) of reionization sources, their star formation rates (SFR), their stellar metallicity and age, the escape fraction of H I ionizing photons produced by each source and the clumping of the intergalactic medium (IGM),

to name a few. A further complication is introduced by supernova feedback and (to a lesser extent) the ultraviolet background (UVB) built up during reionization in suppressing the gas content (and hence star formation) in low-mass galaxies which are the main sources of H I ionizing photons (see e.g. Barkana & Loeb 2001; Ciardi & Ferrara 2005; Maio et al. 2011; Sobacchi & Mesinger 2013; Wyithe & Loeb 2013; Dayal et al. 2015, and references therein).

Lyman Alpha ($\text{Ly}\alpha$) photons are a powerful tool in understanding the ionization state of the IGM given their high optical depth (τ) to H I (e.g. Madau & Rees 2000)

$$\tau = 1.5 \times 10^5 h^{-1} \Omega_m^{-1} \frac{\Omega_b h^2}{0.019} \left(\frac{1+z}{8} \right)^{3/2} (1 + \delta_H) \chi_{\text{HI}}, \quad (1)$$

where h is the Hubble parameter, Ω_b and Ω_m represent the cosmic baryon and matter density, respectively, $(1 + \delta_H)$ is

* E-mail: ahutter@aip.de

the hydrogen over-density and χ_{HI} is the fraction of neutral hydrogen. As seen from this equation, even a neutral hydrogen fraction as low as 10^{-5} can lead to a significant attenuation of Ly α photons at high- z , making them extremely sensitive probes of H I in the IGM. As a result, a class of high- z galaxies called Lyman Alpha Emitters (LAEs), detected by means of their Ly α line (at 1216 Å in the rest frame), have become popular probes of reionization, with statistically significant samples available in the reionization epoch, at $z \simeq 5.7$ and 6.6 (Malhotra et al. 2005; Taniguchi et al. 2005; Shimasaku et al. 2006; Hu et al. 2010; Kashikawa et al. 2006; Ouchi et al. 2010; Kashikawa et al. 2011). Indeed, a number of theoretical papers have used semi-analytic (e.g. Dijkstra et al. 2007; Dayal et al. 2008; Samui et al. 2009) or numerical (e.g. McQuinn et al. 2007; Iliev et al. 2008; Dayal et al. 2011; Forero-Romero et al. 2011; Duval et al. 2014; Hutter et al. 2014) models to reproduce the observed number counts of LAEs (the Ly α luminosity function; LF) at various redshifts in the reionization epoch. However interpreting a change in the Ly α LF is rendered challenging by the fact that the observed Ly α luminosity depends on: (a) the fraction of H I ionizing photons ($1-f_{\text{esc}}$) produced by a galaxy that are able to ionize the interstellar H I resulting in the Ly α recombination line, with the rest (f_{esc}) escaping to ionize the IGM, (b) the fraction of the intrinsic Ly α photons that can emerge out of the galactic environment unattenuated by dust (f_{α}) and H I and (c) the fraction of these emergent Ly α photons that are transmitted (T_{α}) through the IGM (depending on $\langle\chi_{HI}\rangle$) and reach the observer.

Given these uncertainties, we require an alternative measurement to constrain the ionization state using LAEs. One such strong measure is provided by the two-point angular correlation function (ACF) of LAEs that describes their spatial clustering. Indeed, McQuinn et al. (2007) have shown that the spatial clustering can hardly be attributed to anything other than the large scale (\sim Mpc scale) ionization regions created during reionization. This result is similar to that obtained by Jensen et al. (2014) who find that upcoming large-field LAE surveys should be able to detect the clustering boost for sufficiently high global IGM neutral fractions (20% at $z = 6.5$), although Jensen et al. (2013) point out that a sample of several thousand objects is needed to obtain a significant clustering signal. Furthermore, Zheng et al. (2010) have shown that Ly α radiative transfer modifies the ratio of observed and intrinsic Ly α luminosities depending on the density and velocity structure of the environment, i.e. LOS (transverse) density fluctuations are suppressed (enhanced), leading to a change in the amplitude of the two-point correlation function compared to the case without the environmental selection effect. However, while Behrens & Niemeyer (2013) have confirmed a correlation between the observed Ly α luminosity and the underlying density and velocity field, they do not find a significant deformation of the two-point correlation function by post-processing hydrodynamical simulations with a Ly α radiative transfer code.

A second probe is presented by the fraction of Lyman Break Galaxies (LBGs) that show Ly α emission: given that the physical properties of LBGs do not evolve in the

150 Myrs between ($z \simeq 6$ and 7, a sudden change in the fraction of LBGs showing Ly α emission could be attributed to reionization (e.g. Stark et al. 2010, 2011; Fontana et al. 2010; Pentericci et al. 2011; Caruana et al. 2014; Faisst et al. 2014; Schenker et al. 2014; Tilvi et al. 2014). However, this interpretation is complicated by caveats including the redshift dependence of the relative effects of dust on Ly α and ultraviolet (UV) continuum photons (Dayal & Ferrara 2012) and the fact that simple cuts in EW and UV luminosity may lead to uncertainties in the LAE number densities (Dijkstra & Wyithe 2012).

Coupling a cosmological SPH simulation snapshot at $z \simeq 6.6$ with a radiative transfer (RT) code (pCRASH) and a dust model, Hutter et al. (2014) have shown that the effects of f_{esc} , f_{α} and T_{α} are degenerate on the LAE visibility: reproducing the observed Ly α LFs can not differentiate between a Universe which is either completely ionized or half neutral ($\langle\chi_{HI}\rangle \simeq 0.5 - 10^{-4}$), or has an f_{esc} ranging between 5-50%, or has dust that it either clumped or homogeneously distributed in the interstellar medium (ISM) with $f_{\alpha}/f_c = 0.6 - 1.8$; here f_c represents the fraction of UV photons that emerge out of the ISM unattenuated by dust. In this work, we extend our calculations to use the two-point LAE ACF to narrow down the 3-dimensional parameter space of $\langle\chi_{HI}\rangle$, f_{esc} and f_{α}/f_c . Further, we study the time evolution of both the Ly α and UV luminosities to show the *fraction* of time during the past 100 Myrs prior to $z = 6.6$ that a galaxy is visible as a LBG or as a LBG with Ly α emission, both considering the *intrinsic* and *observed* (dust and IGM-attenuated) luminosities. In principle, the ratio of these fractions could be measured by relating the number of observed LBGs with Ly α emission to the number of observed LBGs at $z = 6.6 - 7.3$.

The cosmological model corresponds to the Λ CDM Universe with dark matter (DM), dark energy and baryonic density parameter values of $(\Omega_{\Lambda}, \Omega_m, \Omega_b) = (0.73, 0.27, 0.047)$, a Hubble constant $H_0 = 100h = 70\text{kms}^{-1}\text{Mpc}^{-1}$, and a normalisation $\sigma_8 = 0.82$, consistent with the results from WMAP5 (Komatsu et al. 2009).

2 THE MODEL

In this section we briefly describe our physical model for high-redshift LAEs that couples cosmological SPH simulations run using GADGET-2 with a RT code (pCRASH, Partl et al. (2011)) and a dust model, and interested readers are referred to Hutter et al. (2014) for a detailed description.

The hydrodynamical simulation analysed in this work was carried out with the TreePM-SPH code GADGET-2 and has a box size of $80h^{-1}$ comoving Mpc (cMpc) and contains 1024^3 DM particles, and initially the same number of gas particles; the mass of a DM and gas particle is $3.6 \times 10^7 h^{-1} M_{\odot}$ and $6.3 \times 10^6 h^{-1} M_{\odot}$, respectively. The simulation includes all the standard processes of star formation and its associated metal production and feedback using the prescription of Springel & Hernquist (2003), assuming a Salpeter (Salpeter 1955) initial mass function (IMF) between $0.1 - 100 M_{\odot}$. Bound structures of more than 20 to

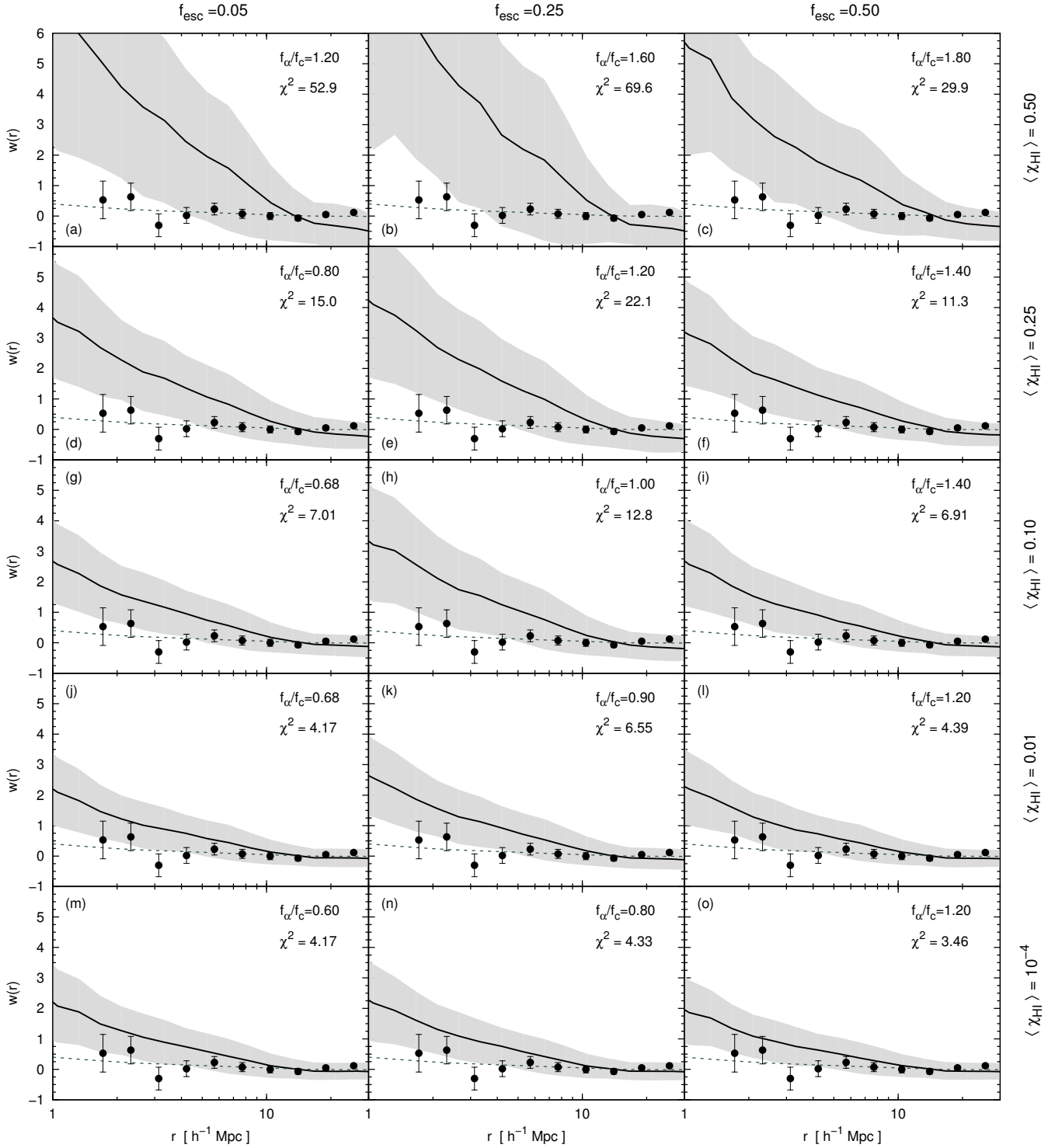


Figure 1. Angular correlation function for simulated LAEs. The mean ACF is calculated from 36 mock catalogues (12 along each of x, y, z directions) assuming volumes with a depth of $30h^{-1}$ Mpc and a FoV of $\sim 3 \times 10^3 h^{-2}$ Mpc². In each panel, the solid line shows the ACF of the best fit ($f_{\alpha}/f_c, f_{esc}, \langle \chi_{HI} \rangle$) combinations for which the simulated LAE Ly α LFs are within the 1σ limit of the observations by Kashikawa et al. (2011) with shaded regions showing the variance across the mock catalogues. In each panel, the grey dashed line shows the ACF for LBGs from the whole box, corresponding errors on the ACF for LBGs are comparable with the line width, and black points represent the observational results by Kashikawa et al. (2006). Columns show the results for $f_{esc} = 0.05, 0.25$ and 0.5 , as marked. The values of $\langle \chi_{HI} \rangle$ are marked at the end of each row, with the f_{α}/f_c value marked in each panel, along with the χ^2 error.

tal (Dark Matter, gas and star) particles are recognised as galaxies using the Amiga Halo Finder (AHF; Knollmann & Knebe 2009). Of all these galaxies, we only use “resolved” galaxies that are complete in the halo mass function in all our calculations - these consist of at least 160 (10) gas (star) particles and have a halo mass $M_h \gtrsim 10^{9.2} M_\odot$. Assuming each star particle to have formed in a burst, we calculate its spectra, and rest-frame intrinsic Ly α (L_α^{int}) and UV continuum ($L_{\lambda,c}^{int}$; 1505Å) luminosities depending on the stellar mass, age and metallicity using the population synthesis code STARBURST99 (Leitherer et al. 1999). For each galaxy, the dust mass and its corresponding UV attenuation are calculated using the dust model described in Dayal et al. (2011). The observed UV specific luminosity is then calculated as $L_{\lambda,c}^{obs} = f_c \times L_{\lambda,c}^{int}$ where f_c is the fraction of UV photons that emerge out of the ISM unattenuated by dust which is fixed by matching to the observed evolving UV LF at $z \simeq 6 - 8$; galaxies with an absolute UV magnitude $M_{UV} \lesssim -17$ are then identified as LBGs. The observed Ly α luminosity (L_α^{obs}) is then calculated as $L_\alpha^{obs} = f_\alpha T_\alpha L_\alpha^{int}$ where f_α and T_α account for dust attenuation in the ISM and by H I in the IGM, respectively. Galaxies with $L_\alpha^{obs} \geq 10^{42}$ erg s $^{-1}$ and $EW = L_\alpha^{obs}/L_{\lambda,c}^{obs} \geq 20$ Å are identified as LAEs.

Given that both L_α^{int} and $\langle \chi_{HI} \rangle$ depend on the fraction of H I ionizing photons that can escape out of the ISM (f_{esc}), we use five values of $f_{esc} = 0.05, 0.25, 0.5, 0.75, 0.95$ to post-process the $z \simeq 6.6$ snapshot of the hydrodynamical simulation with the 3D radiative transfer (pCRASH). To explore the full range of $\langle \chi_{HI} \rangle$ (that determines T_α) we run pCRASH starting from a completely neutral to a completely ionized state and obtain ionization fields for different values of the mean fraction of neutral hydrogen $\langle \chi_{HI} \rangle$; for each galaxy we assume the initial line profile to be Gaussian and compute the average Ly α transmissions along 48 different lines of sight (LOS). For each combination of f_{esc} and $\langle \chi_{HI} \rangle$ the transmission T_α is then fixed and the only free parameter that can be adjusted to match Ly α luminosities to observations is the relative escape fraction of Ly α and UV photons from the ISM, $p = f_\alpha/f_c$.

From the Ly α LFs we find the following trends: the amplitude of the LAE Ly α LF decreases with increasing f_{esc} due to a decrease in L_α^{int} . However, this decline can be compensated by an increase in either f_α/f_c or T_α (in an increasingly ionized IGM). Comparing our model Ly α LFs to observations (Kashikawa et al. 2011) we found that allowing for clumped dust ($p \gtrsim 0.7$), the observations can be reproduced for $\langle \chi_{HI} \rangle \simeq 0.5 - 10^{-4}$, $f_{esc} \simeq 0.05 - 0.5$ and $f_\alpha/f_c = 0.6 - 1.8$ within a 1σ error.

3 CONSTRAINTS FROM LAE CLUSTERING

Given the sensitivity of Ly α photons to H I, the ionization field should be imprinted in the spatial distribution of the LAEs which can be quantified by the two point correlation functions (ACF). In this section, we use the ACF of theoretical LAEs for each of these best-fit combinations (that match the Ly α LF to within a $1-\sigma$ error as summarised in Table 1)

Table 1. For the $\langle \chi_{HI} \rangle$ value shown in Column 1, we summarise the f_α/f_c ratio required to best fit the simulated Ly α LF to observations (Kashikawa et al. 2011) within 1σ limits in columns 2-4 with subscripts showing the f_{esc} value used (Hutter et al. 2014).

$\langle \chi_{HI} \rangle$	$\langle f_\alpha/f_c \rangle_{0.05}$	$\langle f_\alpha/f_c \rangle_{0.25}$	$\langle f_\alpha/f_c \rangle_{0.5}$
0.50	1.2	1.6	1.8
0.25	0.8	1.2	1.4
0.10	0.68	1.0	1.4
0.01	0.68	0.9	1.2
10^{-4}	0.60	0.8	1.2

to narrow the joint constraints on $\langle \chi_{HI} \rangle$, f_{esc} and f_α/f_c . We start by describing our procedure for obtaining LAE ACFs, which depends both on the depth along the LOS (Peebles 1980) since all galaxies are projected to a plane perpendicular to the LOS, as well as the chosen field of view (FoV), which should be comparable to that observed (Kashikawa et al. 2006). Indeed, while the measured ACF should be independent of the FoV if large enough areas are sampled, the restricted observational FoV leads to an ACF that is not independent of sample variance. To get an estimate of the average ACF and its variance, we generate 36 mock catalogues (12 along each of x, y, z directions) for over-lapping volumes comparable to that observed by Kashikawa et al. (2006), corresponding to a redshift distance $\Delta z \sim 0.1$ at $z \simeq 6.5$ and a field of view (FoV) of $\sim 3 \times 10^3 h^{-2} \text{Mpc}^2$. Using the Landy-Szalay estimator we compute the ACF in each mock survey region denoted by $w_i(r)$ with respect to the mean LAE number density \bar{n} of the complete simulation box and estimate the mean value of $w(r)$ as well as its variance from our mock catalogues as

$$\bar{n}(1 + w(r)) = \frac{1}{N} \sum_{i=1}^N n_i(1 + w_i(r)) \quad (2)$$

We start by calculating the LBG ACF (over the entire box) to get an estimate of the underlying galaxy population. As seen from Fig. 1, LBGs are almost homogeneously distributed and the ACF is consistent with essentially no clustering on scales $\lesssim 30h^{-1}$ Mpc. On the other hand, the LAE ACF is affected both by ISM dust, as well as the large scale topology of reionization. It might be expected that in the early stages of reionization, only those galaxies that are clustered and hence capable of building large H II regions would be visible as LAEs (leading to a large amplitude of the ACF), with the amplitude of the ACF decreasing as reionization progresses and faint objects are able to transmit enough flux through the IGM to be visible as LAEs. Indeed, as shown in Fig. 1, LAEs exhibit precisely this behaviour. For a given f_{esc} value (we remind the reader this corresponds to a fixed L_α^{int}), as the IGM becomes more ionized (going down the vertical columns in the Fig. 1), smaller galaxies are able to transmit more of their flux through the IGM, requiring lowering f_α/f_c values to fit the Ly α LF. While for a half neutral IGM (panel a), only strongly clustered galaxies are visible as LAEs ($w(r) \simeq 4.5$) at scales of $\simeq 2h^{-1} \text{Mpc}$, T_α increases for a completely ionized IGM at

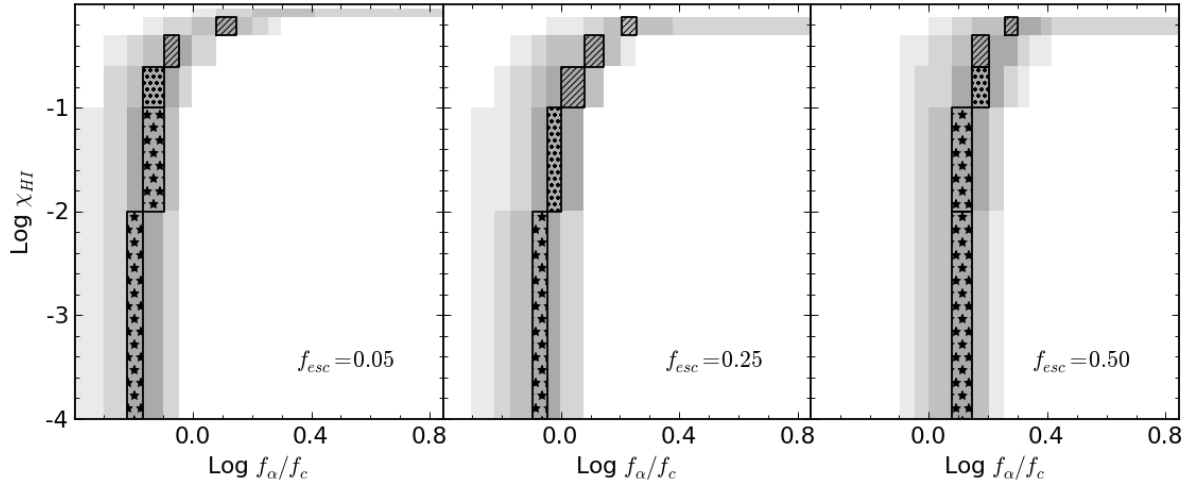


Figure 2. The grey shaded regions show the $(1-5)\sigma$ (dark grey to white respectively) regions for the combinations of f_{esc} , $\langle\chi_{HI}\rangle$ and f_{α}/f_c that best fit the observed Ly α LF data from Hutter et al. (2014). We over-plot black contours for 3σ (stars), 5σ (dots), $> 5\sigma$ (hatching) by comparing model results to observed ACF data Kashikawa et al. (2006). As shown, LAE clustering observations (3σ) require an IGM that has $\chi_{HI} \lesssim 0.01$, $f_{\alpha}/f_c \leq 1.2$ and $f_{esc} \leq 0.5$. See Sec. 3 for details.

the same scale, leading to a more homogeneous LAE distribution resulting in a lower amplitude of the ACF (panel m; $w(r) \simeq 1.5$).

At a given value of $\langle\chi_{HI}\rangle$, L_{α}^{int} decreases with increasing f_{esc} (horizontal rows in the same figure) which must be compensated by an increase in f_{α}/f_c . However, this compensation results in very similar ACFs at a given $\langle\chi_{HI}\rangle$ value. Our results therefore show that the ACF is driven by the reionization topology (as determined by $\langle\chi_{HI}\rangle$), with f_{esc} and the local f_{α}/f_c having a marginal effect (a factor of about 1.5) on its amplitude.

We then calculate the χ^2 errors between our simulated ACFs and observations, and find that observations constrain $\langle\chi_{HI}\rangle \lesssim 0.01$ for $f_{esc} = 0.05, 0.5$ and $\langle\chi_{HI}\rangle \lesssim 10^{-4}$ for $f_{esc} = 0.25$ (to within a 3σ error). Further, while the f_{α}/f_c ratio is compatible with homogeneously distributed dust for $f_{esc} = 0.05$, the decrease in L_{α}^{int} requires clumped dust ($f_{\alpha}/f_c \geq 0.7$) for $f_{esc} = 0.25$ and 0.5 .

To highlight the importance of the spatial clustering of LAEs, we show the $(1-5)\sigma$ constraints allowed by matching the Ly α LFs to observations in Fig. 2. As seen, these encompass a region such that $\langle\chi_{HI}\rangle \simeq 10^{-4} - 0.5$, $f_{esc} = 0.05 - 0.5$ and $f_{\alpha}/f_c = 0.6 - 1.8$. However, building ACFs for each of these allowed combinations, we find that theory and observations yield much tighter constraints of $\langle\chi_{HI}\rangle \simeq 0.01 - 10^{-4}$, $f_{esc} = 0.05 - 0.5$ and $f_{\alpha}/f_c = 0.6 - 1.2$ to within a 3σ error.

Finally, our results show that it is the reionization topology (as parameterised by $\langle\chi_{HI}\rangle$) that drives the ACF, supporting the results obtained by McQuinn et al. (2007), Jensen et al. (2013) and Jensen et al. (2014). Although Jensen et al. (2014) have assumed a simple scaling down of the L_{α} luminosity of all galaxies by a fixed amount due to galaxy evolution, they also find that galaxies are more likely to be observed as LAEs if they reside in ionized re-

gions for $\langle\chi_{HI}\rangle \gtrsim 20\%$. We note that the number of galaxies we identify as LAEs is similar to within 10% for the different f_{esc} , $\langle\chi_{HI}\rangle$ and f_{α}/f_c combinations, demonstrating that the enhanced LAE clustering in our model can be attributed to an increasing neutral IGM.

We note that the average number of LAEs in our mock catalogues (~ 300) exceeds the number of identified objects in Kashikawa et al. (2006). In order to compare to a complete sample we have considered all galaxies with $L_{\alpha}^{obs} \geq 10^{42} \text{ erg s}^{-1}$ and $EW \geq 20 \text{ \AA}$ as LAEs. Since this luminosity cut may include fainter galaxies than observed, the obtained ACFs represent a lower limit, as the clustering increases for higher luminosity cuts (Jensen et al. 2014). According to Jensen et al. (2013) our galaxy sample size of ~ 300 is sufficient to distinguish a half-ionized from an ionized IGM, but does not provide the necessary sample size of ~ 500 to distinguish $\langle\chi_{HI}\rangle = 0.25$ from $\langle\chi_{HI}\rangle = 1$. However, we have modelled the luminosity of each galaxy according to its stellar population obtained from the hydrodynamical simulation. This makes our results more sensitive to the ionization state of the IGM than Jensen et al. (2013); their clustering signal was reduced by the random scatter they added to the imposed fixed mass-to-light ratio. Hence, in agreement with McQuinn et al. (2007) we find our sample size sufficient to distinguish $\langle\chi_{HI}\rangle = 0.25$ from $\langle\chi_{HI}\rangle = 10^{-4}$.

4 THE RELATION BETWEEN LAES AND LBGS

In this section we show how simulated $z \simeq 6.6$ galaxies build up their stellar mass (M_*), and the time evolution of their UV and Ly α luminosities, and Ly α equivalent widths (EW). We then present the fraction of time during the last

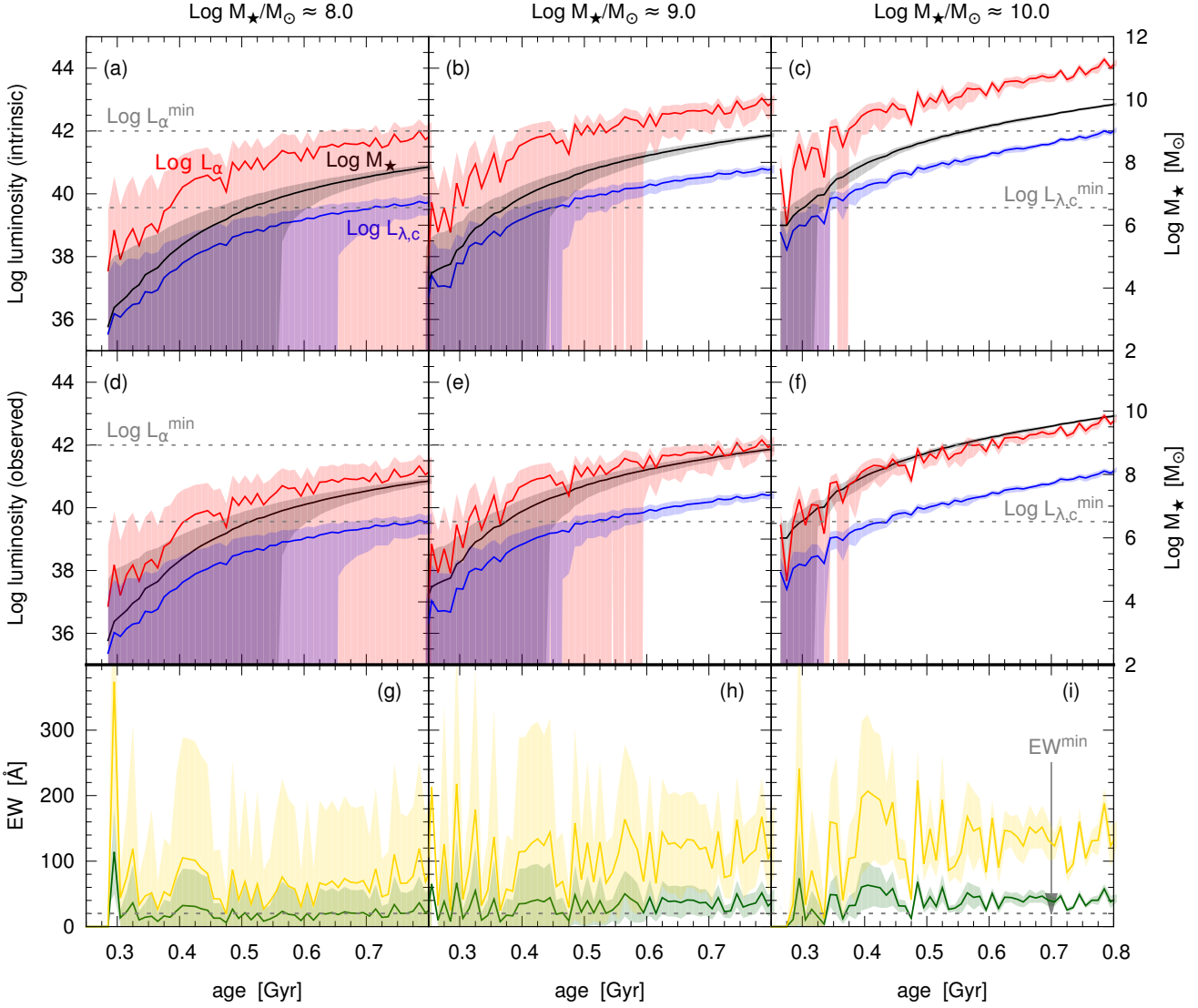


Figure 3. Time evolution of M_* , Ly α and UV luminosities and EWs across three M_* bins of 10^8 , 10^9 and $10^{10}M_\odot$ as marked above each column. The upper 3 panels show the intrinsic quantities (M_* in black; L_α^{int} in red (upper line); $L_{\lambda,c}^{int}$ in blue (lower line)); we use $f_{esc} = 0$ for the Ly α luminosity. The middle three panels show the observed quantities (M_* in black; L_α^{obs} in red (upper line); $L_{\lambda,c}^{obs}$ in blue (lower line)) where we assume $T_\alpha = 0.45$, $f_\alpha = 0.68f_c$ and a individual f_c depending on the dust mass of each galaxy. The dashed lines in the top two panels show the current observational limits corresponding to the Ly α (10^{42}erg s^{-1}) and UV ($10^{39.6}\text{erg s}^{-1}/\text{\AA}$) luminosities. The lower 3 panels show the intrinsic (yellow, upper line) and observed (green, lower line) Ly α EWs with the dashed line showing the minimum limit of 20\AA . In each panel shaded regions show the variance in the given M_* bin.

100 Myrs prior to $z = 6.6$ for which galaxies of different UV magnitudes are visible as LBGs or as LBGs with detectable Ly α emission, both considering intrinsic and observed luminosities for each combination of f_{esc} , $\langle\chi_{HI}\rangle$ and f_α/f_c that reproduces the Ly α LF and LAE ACF within 1σ and 3σ respectively. In order to consider a time span independent of resolution effects we have chosen a period of time of 100 Myrs as an interval. We discuss the limiting case, i.e. considering the total lifetime of each galaxy in our simula-

tion as the corresponding period of time, in the Appendix A.

4.1 Time evolution of stellar mass, Ly α and UV luminosities

We use the ages of each star particle to trace the growth of M_* , and the metallicity and time dependent values of the intrinsic UV and Ly α luminosities ($L_{\lambda,c}^{int}$ and L_α^{int} , respectively) and the intrinsic Ly α EW ($= L_\alpha^{int}/L_{\lambda,c}^{int}$) for galaxies

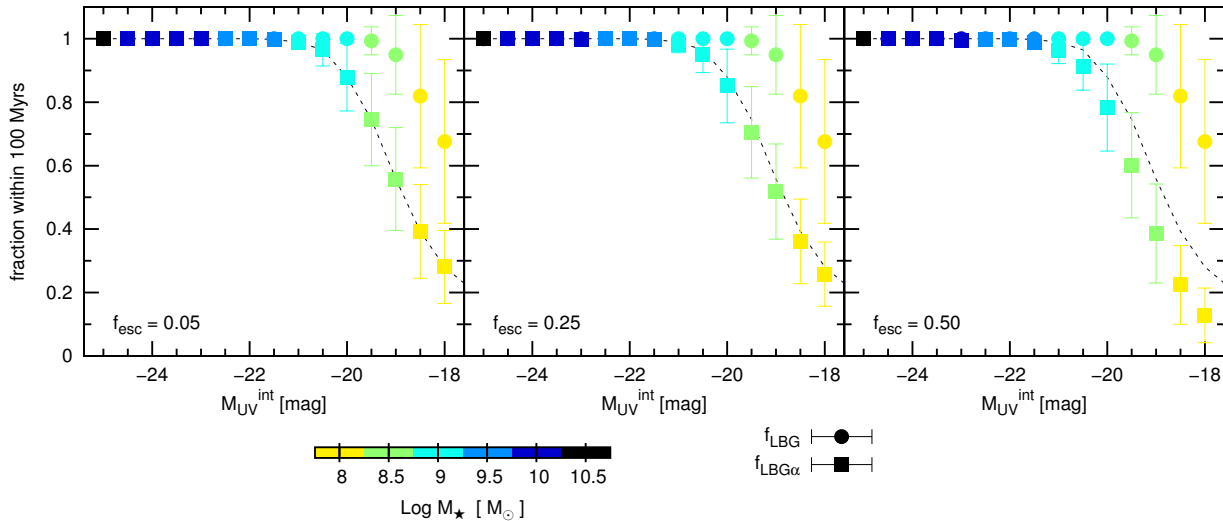


Figure 4. Fraction of time during the last 100 Myrs prior to $z = 6.6$ that galaxies spend as LBGs (f_{LBG} , circles) and as LBGs with a Ly α line ($f_{LBG\alpha}$, squares), as a function of the intrinsic UV luminosity for intrinsic values of Ly α and UV luminosities. The panels show the fractions for the indicated values of $f_{esc} = 0.05, 0.25, 0.5$. The mean stellar mass in each M_{UV} bin is encoded in the shown colour scale. The fractions are computed as the mean of the galaxies within M_{UV} bins k ranging from $k - 0.25$ to $k + 0.25$ for $k = -25 \dots -18$ in steps of 0.5. Error bars show the standard deviations of the mean values. The dotted black line in each panel represents $f_{LBG\alpha}$ for $f_{esc} = 0.05$; as clearly seen, increasing f_{esc} to 0.5, leads to a decrease in $f_{LBG\alpha}$.

in three bins of $M_* \simeq 10^{8,9,10} M_\odot$. We assume that all ionizing photons emitted within galaxies are absorbed in the ISM and produce Ly α radiation, i.e. $f_{esc} = 0$, to investigate the most extreme case.

As seen from the upper three panels of Fig. 3, both $L_{\lambda,c}^{int}$ and L_α^{int} (averaged over the galaxies in the given M_* bin) rise as galaxies steadily build up in (stellar) mass, albeit with a large scatter reflecting the assembly history of different galaxies. As expected for normal star forming galaxies, the average intrinsic Ly α EW for all the three M_* bins considered here has a value between $30 - 300 \text{ \AA}$ (lower 3 panels of the same figure) that is larger than the minimum value of 20 \AA used to identify LAEs. Indeed, we find that once a galaxy exceeds a critical mass of roughly $10^{8.5} (10^{7.5}) M_\odot$, it can produce enough luminosity to intrinsically be a LAE (LBG), it has also met the LBG criterion.

As for observed luminosities, we remind the reader that we compute L_α^{obs} using the fraction of UV photons that escape out of the galaxy (f_c); L_α^{obs} is computed assuming homogeneously distributed dust ($f_\alpha/f_c = 0.68$) and an IGM transmission value of $T_\alpha = 0.45$ (Hutter et al. 2014). As expected, including the effects of dust and the IGM reduces both the Ly α and UV luminosities, as shown in the middle panels of the same figure so that the critical M_* at which a galaxy has the minimum luminosity to be a LAE (LBG) increases to $10^{9.5} (10^{8.5}) M_\odot$, although in most cases the observed EW is still larger than the minimum required value of 20 \AA (bottom most panels).

As expected from our discussion above, the time a galaxy spends as a LBG or LAE increases with increasing M_* . However, in our model a galaxy becomes a LBG before it also turns into a LAE because of the more strin-

gent (luminosity + EW) constraints imposed on identifying a galaxy as a LAE, as expected from the critical M_* values quoted above. To quantify, while galaxies with stellar masses of $\sim 10^8 M_\odot$ are visible as LBGs for roughly the last 80 Myrs, they do not meet the selection criterion to be visible as LAEs: although their intrinsic EW are larger than the minimum value of 20 \AA required by observations (bottom panel of same figure), L_α^{int} does not meet the required Ly α luminosity of $10^{42} \text{ erg s}^{-1}$. Galaxies with $M_* \gtrsim 10^9 M_\odot$ are massive enough to sustain star formation and maintain $L_{\lambda,c}^{int}$ and L_α^{int} values above the required limits. Again, the lifetime spent as a LAE is driven by L_α^{int} , with the intrinsic EW always exceeding 20 \AA (bottom panel of Fig. 3).

When considering observed luminosities, the time a galaxy is visible as a LBG decreases; the decrease is more pronounced for LAEs that are additionally affected by IGM transmission. From panels (d)-(f) of Fig. 3, we see that in addition to galaxies with $10^8 M_\odot$, galaxies with $M_* \simeq 10^9 M_\odot$ are also no longer visible as LAEs as a result of the Ly α luminosity dropping below visible limits.

4.2 The fraction of time spent as LBG and as LBG with Ly α emission

We now calculate the fraction of time during the last 100 Myrs prior to $z = 6.6$ that galaxies in different UV magnitude bins spend as a LBG (f_{LBG}) and as a LBG with Ly α emission ($f_{LBG\alpha}$, i.e. as a LAE), and discuss the resulting fractions ($f_{LBG\alpha}$ and f_{LBG}) for galaxies of varying UV magnitudes $M_{UV} = -18$ to -25 in more detail. We start with intrinsic UV luminosities as shown in Fig. 4: firstly, as galaxies become more massive, they are able to sustain

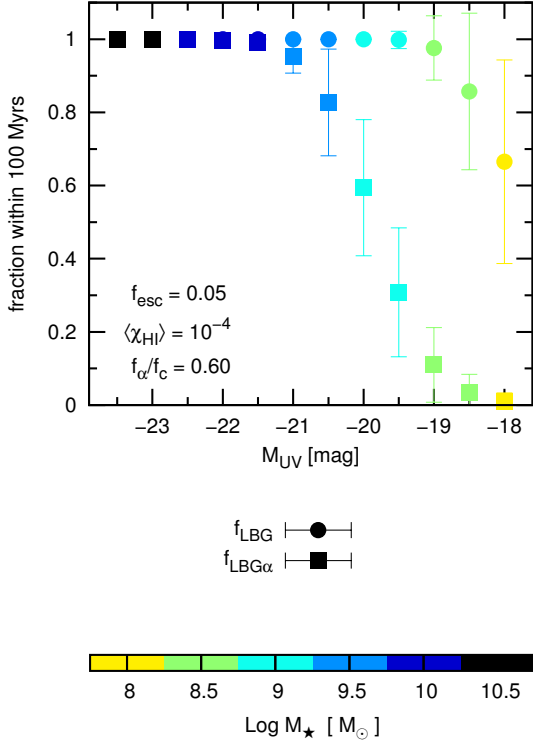


Figure 5. Fraction of time during the last 100 Myrs prior to $z = 6.6$ that galaxies spend as LBGs (f_{LBG} , circles) and as LBGs with a Ly α line ($f_{LBG\alpha}$, squares) as a function of the UV luminosity for our best fit models. The mean stellar mass in each M_{UV} bin is encoded in the shown colour scale. This panel shows the best fit case for $f_{esc} = 0.05$, $\langle \chi_{HI} \rangle = 10^{-4}$ and $f_{\alpha}/f_c = 0.60$. The fractions are computed as the mean of the galaxies within M_{UV} bins k ranging from $k - 0.25$ to $k + 0.25$ for $k = -25 \dots -18$ in steps of 0.5. Error bars show the standard deviations of the mean values. The independence of $f_{LBG\alpha}$ on the chosen best fit model clearly shows that the effects of f_{esc} , $\langle \chi_{HI} \rangle$ and f_{α}/f_c are degenerate on $f_{LBG\alpha}$.

large rates of star formation, leading to M_{UV} values that scale with M_* . Secondly, we find that both f_{LBG} and $f_{LBG\alpha}$ increase with an increase in the UV magnitude (or M_*), as explained in Sec. 4.1 above: f_{LBG} increases from 65% to 100% as M_* increases from $10^8 - 10^{10.5} M_{\odot}$. As a result of the stricter luminosity and EW criterion imposed to identify galaxies as LAEs, $f_{LBG\alpha} < f_{LBG}$ and declines more rapidly than f_{LBG} towards fainter UV luminosities, decreasing from 100% to 10-30% as M_* decreases from $10^{10.5} - 10^8 M_{\odot}$. Further, the decrease in L_{α}^{int} with increasing f_{esc} results in a (linear) decrease in f_{LAE} as shown from panels (a)-(c) of the same figure: while f_{LAE} is comparable for $f_{esc} = 0.05, 0.25$, it decreases by about 0.15 for $f_{esc} = 0.5$, where half of the ionizing photons do not contribute to the Ly α luminosity thereby reducing the fraction of time it shows Ly α emission.

We then calculate f_{LBG} and $f_{LBG\alpha}$ including the effects of dust and IGM attenuation for each of the best-fit parameter combinations that match both the observed Ly α LF and

ACF as shown in Sec. 3. We use the f_c value for each galaxy according to its final dust mass at $z \simeq 6.6$, the Ly α transmission T_{α} of each galaxy was obtained from the ionization field and the ratio of the escape fractions of Ly α and UV continuum photons (f_{α}/f_c) was set according to Table 1. As can be seen from Fig. 5 (since $f_{LBG\alpha}$ is nearly identical for all best fit cases, we show only one best fit case) the additional attenuation by dust in the ISM and neutral hydrogen in the IGM leads to a rise of the mean stellar mass in each M_{UV} bin, as well as to lower values for $f_{LBG\alpha}$ (compared to the intrinsic case) but not for f_{LBG} . Nevertheless, we find the same trends as when considering intrinsic luminosities: f_{LBG} always exceeds $f_{LBG\alpha}$, and f_{LBG} and $f_{LBG\alpha}$ decrease towards fainter UV luminosities with $f_{LBG\alpha}$ declining more rapidly. However the relative difference between f_{LBG} and $f_{LBG\alpha}$ is larger and the decline of $f_{LBG\alpha}$ is more rapid: while f_{LBG} decreases from 100% to 65% as M_{UV} increases from -23.5 to -18.5, $f_{LBG\alpha}$ drops from 100% to essentially 0 for the same magnitude range. The stronger decline in $f_{LBG\alpha}$ is not only due to the additional dust- and IGM attenuation of the Ly α luminosities, but also due to the additional selection criterion in Ly α equivalent width which becomes more important towards UV fainter galaxies.

We also find that the decrease in f_{esc} is compensated by the increase in f_{α}/f_c , leading to very similar $f_{LBG,\alpha}$ ratios for all the models; note that the IGM is almost ionized in most cases, leading to similar T_{α} values. This clearly shows that $\langle \chi_{HI} \rangle$, f_{esc} and f_{α}/f_c compensate each other (as shown in Hutter et al. 2014), as a result of which $f_{LBG\alpha}$ only depends on the combination of the parameters but not on their individual values.

Thus in our model, the most luminous (massive) LBGs most often show Ly α emission, irrespective of whether intrinsic or observed luminosities are considered.

5 DISCUSSION & CONCLUSIONS

We couple a cosmological hydrodynamical simulation (GADGET-2) with a dust model and a radiative transfer code (pCRASH) to model high- z LAEs. Starting from a neutral IGM, we run pCRASH until the IGM is completely ionized, for f_{esc} values ranging from 0.05 to 0.95. In Hutter et al. (2014), we showed that comparing model results to Ly α LF observations simultaneously constrains the escape fraction of ionizing photons f_{esc} , the mean amount of neutral hydrogen $\langle \chi_{HI} \rangle$ and the ratio of the escape fractions of Ly α photons and UV continuum photons f_{α}/f_c to $\langle \chi_{HI} \rangle \simeq 10^{-4} - 0.5$, $f_{esc} = 0.05 - 0.5$ and $f_{\alpha}/f_c = 0.6 - 1.8$. In this paper, we calculate the ACFs for these different combinations and find that comparing these to observations significantly narrows the allowed 3D parameter space (within a 3σ error) to $\langle \chi_{HI} \rangle \simeq 0.01 - 10^{-4}$, $f_{esc} = 0.05 - 0.5$ and $f_{\alpha}/f_c = 0.6 - 1.2$. While the effects of these three parameters are degenerate on the Ly α LFs, the ACF is most sensitive to large-scale ionization topologies and reionization leaves clearly distinguishable ACF imprints (boosting up the strength of the ACF) that can not be compensated by varying f_{esc} or f_{α}/f_c . Further, the ACF allows us to constrain $\langle \chi_{HI} \rangle \leq 0.01$, inde-

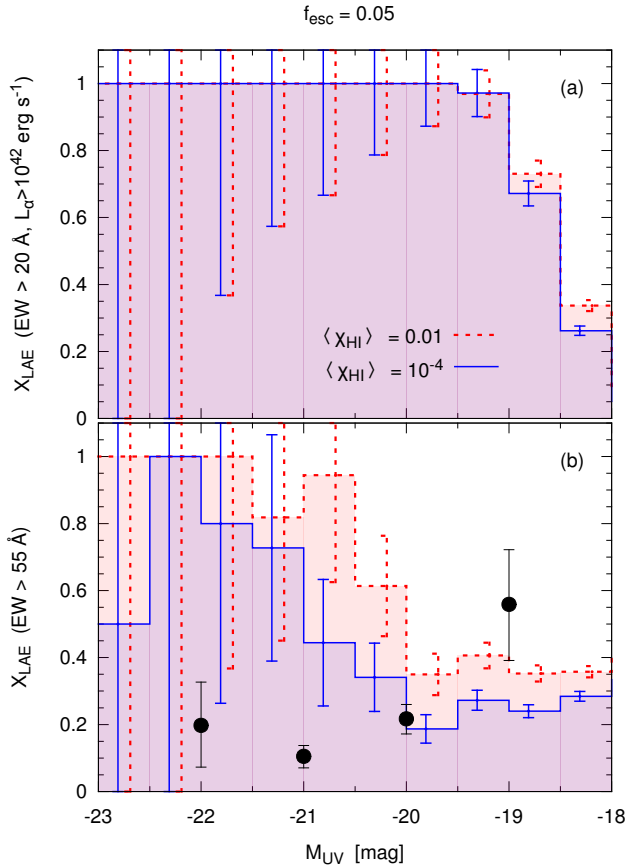


Figure 6. Fraction of LBGs detected also as LAE (X_{LAE}) as a function of UV luminosity. The fractions are shown for fiducial best fit models of $f_{esc} = 0.05$: $\langle \chi_{HI} \rangle = 0.01$, $f_{\alpha}/f_c = 0.68$ (red dashed) and $\langle \chi_{HI} \rangle = 10^{-4}$, $f_{\alpha}/f_c = 0.60$ (blue solid). Error bars are derived from the Poissonian errors of the LAE and LBG numbers. The upper panel (a) shows the fraction X_{LAE} for a LAE selection criterion of $L_{\alpha} > 10^{42} \text{ erg s}^{-1}$ and $EW > 20 \text{ \AA}$, and the lower panel (b) adopts an selection criterion of $EW > 55 \text{ \AA}$, which is in agreement with the observations by Stark et al. (2010). Black points represent the observational constraints of Stark et al. (2010) at $4.5 < z < 6.0$.

pendent of the other two parameters, and we also constrain $f_{esc} \leq 0.5$ and $f_{\alpha}/f_c \leq 1.2$.

We then analyse the average time evolution of UV and Ly α luminosities of simulated galaxies at $z \simeq 6.6$ in three bins of $M_* = 10^{8.9, 9.10} M_{\odot}$, finding the following: as soon as a galaxy exceeds a critical stellar mass of $M_* \simeq 10^{8.5} (10^{7.5}) M_{\odot}$, its intrinsic Ly α (UV) luminosity is large enough for it to be identified as a LAE (LBG). Including the effects of dust and IGM attenuation naturally results in an increase in this critical mass to $10^{9.5}$ and $10^{8.5} M_{\odot}$ for LAEs and LBGs respectively.

Considering the fraction of time during the last 100 Myrs (prior to $z = 6.6$) a galaxy spends as a LBG with Ly α emission ($f_{LBG\alpha}$) or as a LBG (f_{LBG}), we find that the former is always smaller due to the more stringent luminos-

ity and EW constraints imposed on identifying galaxies as LAEs. We find that both the intrinsic and dust-attenuated fraction $f_{LBG\alpha}$ and f_{LBG} rise with increasing UV luminosity (and hence M_*): intrinsically, f_{LBG} ($f_{LBG\alpha}$) increases from 65% to 100% (10-30% to 100%) as M_* increases from $10^8 - 10^{10.5} M_{\odot}$. As expected, including the effects of dust and IGM transmission reduces the values for $f_{LBG\alpha}$ such that $f_{LBG\alpha}$ decreases from 100% to essentially 0 as M_* decreases from $10^{10.5} - 10^8 M_{\odot}$. Finally, we find that the fraction $f_{LBG\alpha}$ of all our models that reproduce the observed Ly α LF and LAE ACFs are independent of the chosen set of parameters: a larger f_{α}/f_c compensates a decrease in T_{α} , or an increase in f_{esc} . As a result, $f_{LBG\alpha}$ only depends on the combination of these 3 parameters but not on their individual values. Thus, it is most often the most luminous LBGs that are visible in the Ly α .

Finally, we summarise the major caveats involved in this study. Firstly, given the cosmological volumes probed by the simulation, we are unable to resolve Lyman Limit systems (LLS) which could lead to a further decrease in the transmission T_{α} along lines of sight (LOS) intercepted by such systems (Bolton & Haehnelt 2013). However, whether LLS are preferentially located in clustered regions, leading to an increasing suppression of T_{α} for massive galaxies remains an open question.

Secondly, as a natural consequence of simulating cosmological volumes we are unable to resolve the ISM of individual galaxies, for which reason we assume a Gaussian profile (with a width set by the rotation velocity of the galaxy) for the Ly α line that emerges out of any galaxy which is probably an unrealistic scenario (see e.g. Verhamme et al. 2008). We note that our constraint on the ionization state of the IGM is model dependent, since the IGM Ly α transmission is sensitive to the the assumed line profile (Jensen et al. 2013).

Thirdly, we assume dust attenuation and IGM transmission to be equal to the values at $z \simeq 6.6$ in order to calculate both $f_{LBG\alpha}$ and f_{LBG} . While the dust mass (and hence attenuation) would be expected to be lower at earlier times, tracing this buildup would require tracking the dust growth in the progenitors of our simulated galaxies. This is beyond the scope of our present paper and we defer to this analysis to a work that is in preparation. Fourthly, $f_{LBG\alpha}$ would be expected to decrease with increasing z as a result of an increase in $\langle \chi_{HI} \rangle$ (leading to a decrease in T_{α}). However, properly accounting for the latter effect requires modelling the entire history of reionization.

While we have explored the full range of possible values for f_{esc} , its mass and z -dependence remain poorly understood, which is also one of the main caveats involved in modelling the time-evolution of reionization. An increase in f_{esc} with decreasing mass (Ferrara & Loeb 2013, e.g.) would suppress the visibility of low-mass objects, and strongly impact the reionization fields we generate, emphasising the strong clustering of high-mass halos (Kaiser 1984; Bardeen et al. 1986; Mo & White 1996), whilst depressing the LF at the faint end. Bringing these values into agreement with observations would then require an f_{α}/f_c ratio that decreases with increasing mass. With its observations of the ionization

topology, instruments such as LoFAR will be invaluable in answering some of these outstanding questions.

Finally, we calculate the fraction of LBGs that would be identified as LAEs, X_{LAE} . Imposing a LAE selection criterion of $L_\alpha \geq 10^{42} \text{ erg s}^{-1}$ and $EW \geq 20 \text{ \AA}$ we find that it is the faintest LBGs that do not show Ly α emission (cf. Dayal & Ferrara 2012), while all LBGs brighter than $M_{UV} \sim -20$ are identified as LAEs at $z \simeq 6.6$ (see Fig. 6). Even if the Ly α selection criterion is made more stringent, i.e. $EW > 55 \text{ \AA}$, X_{LAE} does not show the behaviour observed by Stark et al. (2010), increasing instead of decreasing with UV magnitude. This mis-match is probably due to a combination of the following effects: firstly, the Ly α IGM transmission (T_α) is subject to a large variance along different lines of sight (LOS) (see Hutter et al. 2014) due to the patchy nature of reionization; while we use T_α values averaged over 48 LOS, using values along a specific LOS would lead to an over- or underestimate of T_α . Secondly, as mentioned before, it is possible that the inclusion of LLS could decrease T_α of massive galaxies, leading to lower Ly α EW values respectively. Thirdly, the results by Stark et al. (2010) are based on a post-reionization sample of galaxies ($4.5 < z < 6.0$), while our simulation samples the end of reionization era. The evolution of the UV (and Ly α) LFs of LAEs and LBGs suggest that the emitted observable Ly α radiation varies with cosmic epoch, depending predominantly on the evolution of dust and gas at $z < 6$ and on the IGM neutral hydrogen fraction at $z > 6$. Thus, the probe of LBGs with/without Ly α emission in Stark et al. (2010) (dusty, ionized IGM) may differ to the LBG and LAE population at the end of reionization (less dusty, partly neutral IGM). Indeed, a remarkable high fraction of strong LAEs among $6.0 < z < 6.5$ luminous LBGs ($-21.75 < M_{UV} < -20.25$) (Curtis-Lake et al. 2012) indicates that most LBGs are also identified as LAEs, which is in agreement with our findings. However, their sample suffers from low statistics, which will be overcome by upcoming Subaru/HST/UltraVISTA data. Finally, as an observational caveat, Verhamme et al. (2012) have shown that detailed Ly α radiative transfer calculations of simulated galaxies suggest stronger inclination effects for Ly α photons than for UV continuum photons, introducing biases in the selection function of narrow-band LAE surveys that could lead to a significant fraction of LBGs galaxies being missed as LAEs. We aim at investigating these effects in detail in future works and shedding light on the tantalising connection between LBGs visible/invisible as LAEs.

ACKNOWLEDGEMENTS

The authors thank the anonymous referee for their insightful comments and suggestions that helped to improve the paper, as well as M. Dijkstra, N. Kashikawa, D. Schaerer and P. Creasey for useful discussions. PD acknowledges the support of the Addison Wheeler Fellowship awarded by the Institute of Advanced Study at Durham University.

REFERENCES

- Bardeen J. M., Bond J. R., Kaiser N., Szalay A. S., 1986, ApJ, 304, 15
- Barkana R., Loeb A., 2001, Phys. Rep., 349, 125
- Behrens C., Niemeyer J., 2013, A&A, 556, A5
- Bolton J. S., Haehnelt M. G., 2013, MNRAS, 429, 1695
- Caruana J., Bunker A. J., Wilkins S. M., Stanway E. R., Lorenzoni S., Jarvis M. J., Ebert H., 2014, MNRAS, 443, 2831
- Ciardi B., Ferrara A., 2005, Space Sci. Rev., 116, 625
- Curtis-Lake E. et al., 2012, MNRAS, 422, 1425
- Dayal P., Choudhury T. R., Bromm V., Pacucci F., 2015, ArXiv e-prints 1501.02823
- Dayal P., Ferrara A., 2012, MNRAS, 421, 2568
- Dayal P., Ferrara A., Gallerani S., 2008, MNRAS, 389, 1683
- Dayal P., Maselli A., Ferrara A., 2011, MNRAS, 410, 830
- Dijkstra M., Lidz A., Wyithe J. S. B., 2007, MNRAS, 377, 1175
- Dijkstra M., Wyithe J. S. B., 2012, MNRAS, 419, 3181
- Duval F., Schaerer D., Östlin G., Laursen P., 2014, A&A, 562, A52
- Faisst A. L., Capak P., Carollo C. M., Scarlata C., Scoville N., 2014, ApJ, 788, 87
- Ferrara A., Loeb A., 2013, MNRAS, 431, 2826
- Fontana A. et al., 2010, ApJ, 725, L205
- Forero-Romero J. E., Yepes G., Gottlöber S., Knollmann S. R., Cuesta A. J., Prada F., 2011, MNRAS, 415, 3666
- Hu E. M., Cowie L. L., Barger A. J., Capak P., Kakazu Y., Trouille L., 2010, ApJ, 725, 394
- Hutter A., Dayal P., Partl A. M., Müller V., 2014, MNRAS, 441, 2861
- Iliev I. T., Shapiro P. R., McDonald P., Mellema G., Pen U.-L., 2008, MNRAS, 391, 63
- Jensen H., Hayes M., Iliev I. T., Laursen P., Mellema G., Zackrisson E., 2014, MNRAS, 444, 2114
- Jensen H., Laursen P., Mellema G., Iliev I. T., Sommer-Larsen J., Shapiro P. R., 2013, MNRAS, 428, 1366
- Kaiser N., 1984, ApJ, 284, L9
- Kashikawa N. et al., 2006, ApJ, 648, 7
- Kashikawa N. et al., 2011, ApJ, 734, 119
- Knollmann S. R., Knebe A., 2009, ApJS, 182, 608
- Komatsu E. et al., 2009, ApJS, 180, 330
- Leitherer C. et al., 1999, ApJS, 123, 3
- Madau P., Rees M. J., 2000, ApJ, 542, L69
- Maio U., Khochfar S., Johnson J. L., Ciardi B., 2011, MNRAS, 414, 1145
- Malhotra S. et al., 2005, ApJ, 626, 666
- McQuinn M., Hernquist L., Zaldarriaga M., Dutta S., 2007, MNRAS, 381, 75
- Mo H. J., White S. D. M., 1996, MNRAS, 282, 347
- Ouchi M. et al., 2010, ApJ, 723, 869
- Partl A. M., Maselli A., Ciardi B., Ferrara A., Müller V., 2011, MNRAS, 414, 428
- Peebles P. J. E., 1980, The large-scale structure of the universe
- Pentericci L. et al., 2011, ApJ, 743, 132
- Salpeter E. E., 1955, ApJ, 121, 161
- Samui S., Srianand R., Subramanian K., 2009, MNRAS,

- 398, 2061
 Schenker M. A., Ellis R. S., Konidaris N. P., Stark D. P., 2014, ApJ, 795, 20
 Shimasaku K. et al., 2006, PASJ, 58, 313
 Sobacchi E., Mesinger A., 2013, MNRAS, 432, 3340
 Springel V., Hernquist L., 2003, MNRAS, 339, 289
 Stark D. P., Ellis R. S., Chiu K., Ouchi M., Bunker A., 2010, MNRAS, 408, 1628
 Stark D. P., Ellis R. S., Ouchi M., 2011, ApJ, 728, L2
 Taniguchi Y. et al., 2005, PASJ, 57, 165
 Tilvi V. et al., 2014, ApJ, 794, 5
 Verhamme A., Dubois Y., Blaizot J., Garel T., Bacon R., Devriendt J., Guiderdoni B., Slyz A., 2012, A&A, 546, A111
 Verhamme A., Schaerer D., Atek H., Tapken C., 2008, A&A, 491, 89
 Wyithe J. S. B., Loeb A., 2013, MNRAS, 428, 2741
 Zheng Z., Cen R., Trac H., Miralda-Escudé J., 2010, ApJ, 716, 574

APPENDIX A: THE FRACTION OF LIFETIME SPENT AS LBG WITH AND WITHOUT $\text{Ly}\alpha$ EMISSION

We also show results for the limiting case where the age is the time since the onset of star formation, showing how the fractions of lifetime change when the time span is increased. We take the total age of a galaxy as the time between the formation of the first star and $z = 6.6$, and calculate the corresponding fractions of lifetime that galaxies in different M_{UV} bins spend as a LBG and as a LBG with $\text{Ly}\alpha$ emission (f_{LBG} and $f_{LBG\alpha}$, respectively). As described in Section 4.2, we compute the fractions of lifetime for our best fit models (see Table 1) and show the fractions for the $f_{esc} = 0.5$, $\langle\chi_{HI}\rangle \simeq 0.01$ and f_α/f_c best fit case in Fig. A1. We note that the fractions $f_{LBG\alpha}$ of all other best fit cases are nearly identical to the shown one. Compared to the fractions derived for a time span of 100 Myrs, the fractions of the total lifetime decrease for all UV luminosities. Galaxies that have been identified as LBGs or LBGs with $\text{Ly}\alpha$ emission within 100 Myrs prior to $z = 6.6$ have been fainter at earlier times where they have not met the selection criteria. The decrease in f_{LBG} and $f_{LBG\alpha}$ illustrates the growth of stellar mass in galaxies with time and the existence of a critical stellar mass above which a galaxy produces enough luminosity to be identified as a LBG or as a LBG with $\text{Ly}\alpha$ emission. However, we like to note that the point in time when the first star forms depends on the resolution of the simulation, making our fractions of lifetime resolution-dependent but showing their trends as the time span is increased.

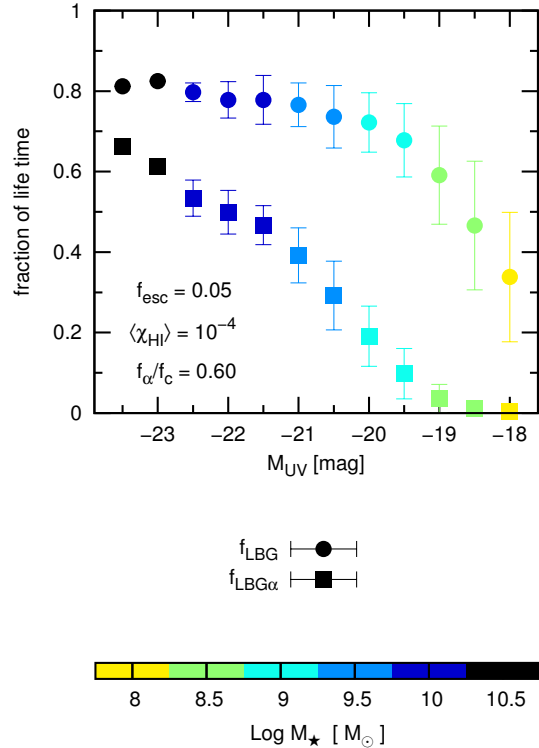


Figure A1. Fraction of lifetime that galaxies spend as LBGs (f_{LBG} , circles) or as LBGs and LAEs ($f_{LBG\alpha}$, squares) as a function of the UV luminosity for our best fit models. The mean stellar mass in each M_{UV} bin is encoded in the shown colour scale. This panel shows the best fit case for $f_{esc} = 0.05$, $\langle\chi_{HI}\rangle = 10^{-4}$ and $f_\alpha/f_c = 0.60$. We omit to show the other best fit cases, since they are nearly identical to the shown one. For each best fit model we assume individual f_c values for each galaxy according to its final dust mass at $z \simeq 6.6$; the $\text{Ly}\alpha$ transmission T_α of each galaxy was obtained from the respective ionization field and the ratio of the escape fractions of $\text{Ly}\alpha$ and UV continuum photons was set according to Table 1. The fractions are computed as the mean of the galaxies within M_{UV} bins k ranging from $k - 0.25$ to $k + 0.25$ for $k = -25 \dots -18$ in steps of 0.5. Error bars show the standard deviations of the mean values.